CFD and Aeroelastic Analysis of the MEXICO Wind Turbine

2014 J. Phys.: Conf. Ser. 555 012006

(http://iopscience.iop.org/1742-6596/555/1/012006)

CFD and Aeroelastic Analysis of the MEXICO Wind Turbine

M. Carrión, M. Woodgate, R. Steijl and G. Barakos

Computational Fluid Dynamics Laboratory, Department of Engineering, University of Liverpool, Harrison Hughes Building, Liverpool, L69 3GH, U.K.

E-mail: g.barakos@liverpool.ac.uk (corresponding author).

S.Gómez-Iradi and X.Munduate

National Renewable Energy Center of Spain, CENER

Abstract. This paper presents an aerodynamic and aeroelastic analysis of the MEXICO wind turbine, using the compressible HMB solver of Liverpool. The aeroelasticity of the blade, as well as the effect of a low-Mach scheme were studied for the zero-yaw $15m/s$ wind case and steady-state computations. The wake developed behind the rotor was also extracted and compared with the experimental data, using the compressible solver and a low-Mach scheme.

It was found that the loads were not sensitive to the Mach number effects, although the low-Mach scheme improved the wake predictions. The sensitivity of the results to the blade structural properties was also highlighted.

1. Introduction

Since the results of the MEXICO project were released [26], several authors have used the data to validate computational methods. The most popular test case is at $15m/s$ wind speed, zero-yaw, and pitch angle of -2.3 degrees. Yawed conditions have also been considered by some authors [37, 34, 35].

Published papers regarding the MEXICO experiment include the work of Bechmann et al. [29], who used the incompressible solver *EllypSys3D*. The isolated three-bladed rotor was considered and better agreement with the pressure distributions was obtained at the outer sections of the blade. The same authors also studied the blade wake, reporting reasonable agreement of the axial velocity component one rotor diameter downstream. Likewise, Shen et al. [31] used the same solver to run the MEXICO rotor inside the wind tunnel, by a combination of an actuator line model and LES computations. To determine the body forces on the rotor blades, they employed a blade element approach combined with 2D aerofoil data, either directly extracted from the experiments or corrected for tip effects [31]. Comparisons of blade loadings showed that the latter technique was in better agreement with the measurements than with the original 2D aerofoil data. In addition, comparisons of detailed near-wake velocities showed good agreement, concluding that tunnel effects were not significant.

Pressure and PIV data were used by Yang et al. [30] to develop a new technique for determining the angle of attack and aerofoil data from the MEXICO blade, by subtracting the induced velocity created by bound circulation from the PIV measurements. The derived aerofoil

data was loaded into a BEM code. The computed loads agreed well with the measurements. However, they found that using the original 2D aerofoil data in the BEM code, the rotor loading was over-predicted, possibly due to strong 3D effects, originating from its complex geometry. Micallef et al. [34] carried out an investigation of the radial velocities close to the rotor plane, using a 3D unsteady potential panel method. They found that radial velocities were higher near the tip region than the root. Likewise, close to the blade, the radial flow velocity is not entirely due to the blade vorticity, but wake-induced radial velocities become important and must be taken into consideration. The computed location of the tip vortices agreed well with the experiments, although the measured tip vortices convected faster downstream. The main discrepancies were concentrated at the mid-span stations. Breton et al. [33] used the PIV data to compare URANS CFD results with the full rotor and an actuator disk model. For this, the vortex position, radius and strength were obtained, with better agreement reported at the near-wake. It was also found that the method employed in the calculation of the radius and strength of the vortices strongly influenced the results and the grid coarseness lead to numerical dissipation, making the identification of vortices difficult.

Xudong et al. [32] implemented a tool for optimising wind turbine blades, consisting of an aeroelastic model and the BEM technique, with a tip-loss correction model. The design variables employed were the chord, twist and relative thickness. Computed aerodynamic results, axial and tangential forces, were compared with MEXICO data with aeroelastic effects accounted for. Flapwise and edgewise deflections were compared between the original and optimised rotors, concluding that the MEXICO blade was near optimal, in terms of the cost for energy production. Only a small correction of the chord near the tip was needed, reducing the cost by further 1.15%.

Pereira et al, [35] adapted the Beddoes-Leishman dynamic stall model for incompressible flows around wind turbines and implemented it into a BEM code. Normal force coefficients at different azimuth angles were compared with the experimental data and better agreement was observed than with the static BEM method, mainly at the sections with higher angles of attack. When large yaw misalignments were considered, the agreement with the experiments was worse.

Table 1 summarises the works on the MEXICO wind turbine. Details of the employed solvers, geometry and flow conditions are given. An indication of whether the pressure (P) and/or the velocity field (PIV) were studied is also given.

All authors have encountered discrepancies between their results and the experiments, mainly for the inner sections of the blade. This puts the reliability of the experimental data into question. However, to date, no aeroelastic effects have been taken into consideration in computations. This is important, since the larger the wind turbines become, the lower their stiffness, and the easier their deformations. Likewise, while at the tip of the blades the local Mach numbers can reach values up to 0.4, at the root they are very low and the compressibility effects may be neglected. That is why the low-Mach effects must be also studied. With regard to the PIV, published papers mainly study the axial flow component.

IOP Publishing
doi:10.1088/1742-6596/555/1/012006

Table 1. Computations of the MEXICO project carried out. *R: Rotor, B: Single blade, N: Nacelle, T: Tower, WT: Wind Tunnel, A: Axial, Y: Yawed, st.: steady, un.: unsteady, AL: Actuator Line, LLT: Lifting Line Theory, FV: Free Vortex, DFW: Direct Free Wake, IFW: Inverse Free Wake, PM: Panel Method, ST: Stall Model, DST: Dynamic Stall Model, pan.: panels, ω: Rotational speed, ϕ: Pitch angle, P: Pressure, PIV: Particle Image Velocimetry, n: no, y: yes., Aeroel.: Aeroelastic method.*

Reported by	Solver	Model	Turbulence Model	Geometry	Mesh size	Flow	ω (rpm)	v_{wind} (m/s)	ϕ $(^\circ)$	P	PIV
Bechman[29]	EllypSys3D	st.RANS	$k-\omega$ SST	R	16M	A	425.5	10,15,24	-2.3	y	y
Yang[30]	-	IFW +BEM	-	B	-	A	[324.4,424.4]	[10,24]	[-5.3,1.7]	y	y
Réthoré[38, 39]	EllypSys3D	st.RANS un.RANS st./un.RANS/DES	$k-\omega$ SST	WT R WT+R	12M 14M 26M	A	-	10,15,24	-2.3	y	y
Grasso[37]	AWSM	LLT + FV	-	R	-	A Y (30°)	-	10,15,24 15	-2.3	n	y
Shen[31]	EllypSys3D	AL/un.LES	-	R WT+R	11.8M 26.2M	A A	424.5	10,15,24	-2.3	y	y
Lutz[36]	FLOWer	st. RANS un.RANS un.RANS	$k-\omega$	R+N R+N R+N+T	17.1M 9.1M 9.1M	A	-	10,15,24	-2.3	n	y
Micallef[40]	-	IFW DFW BEM	-	R	21 elem. 18 elem. -	Y ($^+/_-30°$)	-	15	-2.3	n	y
Micallef[34]	-	un.PM+FV	-	R+N	3908 pan.	A, Y ($^+/_-30°$)	424.5	15	-2.3	n	y
Schreck[41]	-	IFW	-	B	-	A	325	[5.4,30]	-2.3	y	n
Xudong[32]	-	BEM + Aero-elastic	-	R	20 elem.	A	424.5	15,25	-2.3,0.7	y	n
Guntur[42]	-	BEM + 3D ST	-	R	50 elem.	A	425	[5,30]	-2.3	y	n
Breton[33]	- WMB	AS+CVFEM URANS	- $k-\omega$ SST	R R	0.54M 25M	A A	424.5 424.5	10,15,24 10,15,24	-2.3 -2.3	n n	y y
Gómez-Iradi[43]	FAST WMB WMB	BEM+LLT URANS URANS	- $k-\omega$ SST $k-\omega$ SST	R	26 elem. 5.7M 11.5M	A	0	30	[90,-2.3]	y	n
Gómez-Iradi[44]	WMB	URANS	$k-\omega$/SST	NACA64-418 DU91-W2-250	-	-	-	-	-	y	n
Pereira[35]	-	DST+BEM	-	R	15 elem.	Y ($30°, 45°$)	-	24	-2.3	y	n
Current work	HMB	st.RANS+Aeroel. st.RANS	$k-\omega$	R	2.6M 10.2M	A	424.5	15	-2.3	y y	n y

2. Numerical method

2.1. The HMB solver

The Helicopter Multi-Block (HMB) code [1]-[13], developed at Liverpool, is used for the present work. HMB solves the Navier-Stokes equations in integral form using the arbitrary Lagrangian Eulerian (ALE) formulation for time-dependent domains with moving boundaries:

$$\frac{d}{dt}\int_{V(t)} \vec{\mathbf{w}} dV + \int_{\partial V(t)} \left(\vec{F}_i\left(\vec{\mathbf{w}}\right) - \vec{F}_v\left(\vec{\mathbf{w}}\right)\right) \vec{n} dS = \vec{S} \tag{1}$$

where $V(t)$ is the time dependent control volume, $\partial V(t)$ its boundary, $\vec{\mathbf{w}}$ is the vector of conserved variables $[\rho, \rho u, \rho v, \rho w, \rho E]^T$. $\vec{F}_i$ and $\vec{F}_v$ are the inviscid and viscous fluxes, including the effects of the mesh movement. For hovering rotor simulations, the grid is not rotating. A source term $\vec{S} = [0, -\rho\vec{\omega} \times \vec{u}_h, 0]^T$ is however added to compensate for the inertial effects of the rotation along with a velocity assigned to grid nodes. $\vec{u}_h$ is the local velocity field in the rotor-fixed frame of reference.

The Navier-Stokes equation are discretised using a cell-centred finite volume approach on a multi-block grid, leading to the following equations:

$$\frac{\partial}{\partial t}\left(\mathbf{w}_{i,j,k} V_{i,j,k}\right) = -\mathbf{R}_{i,j,k}\left(\mathbf{w}_{i,j,k}\right) \tag{2}$$

where $\mathbf{w}$ represents the cell variables and $\mathbf{R}$ the residuals. i, j and k are the cell indices and $V_{i,j,k}$ is the cell volume. Osher's [21] upwind scheme is used to discretise the convective terms and MUSCL variable interpolation is used for nominally third order accuracy. The Van Albada limiter is used to reduce the oscillations near steep gradients. Temporal integration is performed using an implicit dual-time step method. The linearised system is solved using the generalised conjugate gradient method with a block incomplete lower-upper (BILU) pre-conditioner [15].

HMB solver has a library of turbulence closures which includes several one- and two- equation turbulence models and even non-Boussinesq versions of the $k-\omega$ model. Turbulence simulation is also possible using either the Large-Eddy or the Detached-Eddy approach.

Multi-block structured meshes are used for HMB. These meshes are generated using ICEM-Hexa$^{\text{TM}}$of ANSYS. The multi-block topology allows for an easy sharing of the calculation load for parallel computing. For rotor flows, a typical multi-block topology used in the University of Liverpool is described in [11].

2.2. Aeroelasticity Analysis Method

NASTRAN is used for calculating the static structural deformations of a blade that is modelled as a beam. Non-linear CBEAM elements are used along the quarter-chord line of the blade and contain all the blade structural properties. A non-linear static analysis is performed (SOL 106), taking into account the centrifugal forces. This is followed by an iterative process allowing for the large displacements to be taken into account while recomputing the forces due to the aerodynamic loads and the centrifugal forces at each step. The main structural properties needed for this analysis are the distributions of the sectional area, the chordwise and flapwise area moments of inertia, the torsional constant and the linear mass distribution along the span. The offset between the elastic axis and the centre of gravity along the span can also be added to refine the analysis. All structural properties are linearly interpolated between the ends of the beam element. CBAR elements without any structural properties are also used for interpolating the beam model deformation to the blade surface, which is then used for deforming the fluid grid.

The employed NASTRAN model for the MEXICO blade contains 20 CBEAM elements along the blade span and is shown in Figure 5.

For CFD/CSD coupling, the aerodynamic loads are first extracted from the fluid solution and are then used in NASTRAN to obtain the required blade shape. The blade is then deformed based on the structural shape using the method described below. This process is repeated until convergence.

The method developed for HMB [4] first deforms the blade surface using the Constant Volume Tetrahedron (CVT) method, which projects each fluid node to the nearest structural triangular element and moves it linearly with the element. Then, it obtains the updated block vertex positions via spring analogy (SAM). Finally, it generates the full mesh via Transfinite Interpolation (TFI). The method is described in reference [14], and uses the properties of multi-block meshes to maintain its efficiency as the number of blocks increases, particularly in the spanwise blade direction. It provides flexibility and allows for complex multi-block topologies to be used with good control over the distribution of mesh deformation all over the computational domain.

2.3. All-Mach scheme

To account for low-Mach effects, the Low-Mach Roe scheme (LM-Roe) developed by Rieper [23] was implemented in the HMB solver. For details of the implementation, the reader may refer to [24]. The basic principle of this method is scaling the normal velocity jump at the cell interface, Δu_n, by a function dependent on the local Mach number $f(M)$. The fluxes are calculated as,

$$F_{i+1/2}^{LM-Roe} = \frac{1}{2}(F_i + F_{i+1}) - \frac{1}{2} R_{i+1/2}^{Roe} |\Lambda_{i+1/2}^{Roe}| \alpha_{i+1/2}^{LM-Roe}, \tag{3}$$

where,

$$\alpha_{\mathbf{i+1/2}}^{\mathbf{LM-Roe}} = L_{i+1/2}^{Roe}(Q_{i+1} - Q_i) = \begin{pmatrix} \frac{\Delta p}{2c^2} - \frac{\overline{\rho}}{2c} f(M) \Delta u_n \\ \Delta\rho - \frac{\Delta p}{c^2} \\ \frac{\Delta p}{2c^2} + \frac{\overline{\rho}}{2c} f(M) \Delta u_n \\ \overline{\rho} \Delta u_p \\ \overline{\rho} \Delta u_m \end{pmatrix}. \tag{4}$$

The first term in the right hand side of Equation 3 is the central term, while the second term is the dissipation. $R_{i+1/2}^{Roe}$ and $L_{i+1/2}^{Roe}$ are the right and left eigenvectors, respectively, and $\Lambda_{i+1/2}^{Roe}$ is the matrix of eigenvalues. In Equation 4, u_n is the velocity normal to the cell interface, u_p and u_m are the transverse components. Likewise, $\overline{\rho}$ indicates the Roe-averaged density. The scaling function employed is the one suggested by Li [25]:

$$f(M) \quad = \quad M \frac{\sqrt{4 + (1 - M^2)^2}}{1 + M^2} \tag{5}$$

For Mach numbers up to 0.1 the solution obtained with this scheme and the Osher's solver were almost identical, while improvements are obtained for lower Mach number values. This can be seen in Figure 1, for the pressure distribution and lift and pressure drag convergence of the S809 aerofoil [27] at 2.1 degrees of incidence angle obtained with Osher's and the LM-Roe schemes and compared with the experimental data published in [28].

3. Grid generation

As MEXICO is a three-bladed rotor, only a third of the domain was meshed, see Figure 4, assuming periodicity of the problem. Table 2 lists the employed grids for this study. The blocking employed is based on a C-topology at the leading edge of the blade, while an H-topology is selected at the trailing edge. This optimises the orthogonality of the cells around

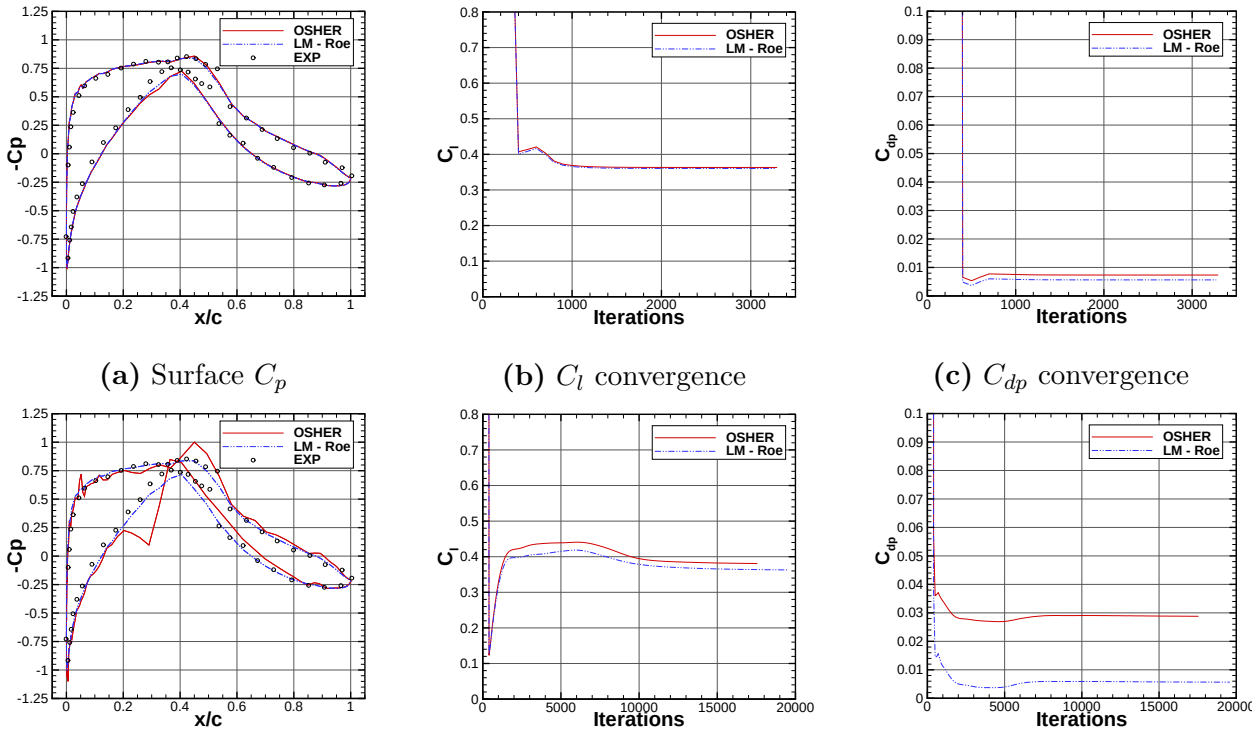

(a) Surface C_p **(b)** C_l convergence **(c)** C_{dp} convergence

(d) Surface C_p **(e)** C_l convergence **(f)** C_{dp} convergence

Figure 1. Comparison of the performance between Osher's [21] and LM-Roe [23] schemes, for the S809 aerofoil at 2.1 degrees of incidence angle. Top: $M_\infty = 0.1$, Bottom: $M_\infty = 0.01$. The Reynolds number is 10^6 and the turbulence model employed is the k-ω. The employed 2D viscous grid has 29,240 cells.

the blade surface, which leads to a better boundary layer resolution (see Figures 2 and 3). The first grid space normal to the blade is $2.4 \cdot 10^{-6}$m, which gives y^+ less than 1.0 all over the blade. In order to be able to apply periodicity at the symmetry plane, a hub approximated as an infinite cylinder is considered in the geometry. Note that grid 2 uses the sliding planes technique, described in [9], for controlling the refinement of the grid in the wake. For this, a configuration of 2 sliding planes parallel to the plane of the rotor was selected, as can be seen in Figure 4.

Table 2. Summary of mesh properties (*I: Inflow, O: Outflow, FF: Far-field*).

Grid	Geometry	Size (Blocks)	Chord-(span-) wise cells	Boundaries in Radii (R)	CPUs
1	Blade & hub	2.6M(169)	160(111)	I:3 O:6 FF:4	12
2	Blade & hub	10.2M(270)	224(176)	I:3 O:6 FF:4	30

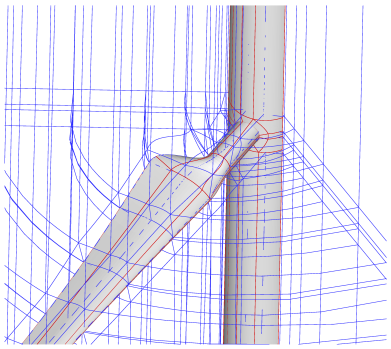

Figure 2. Multi-block topology around the blade and hub.

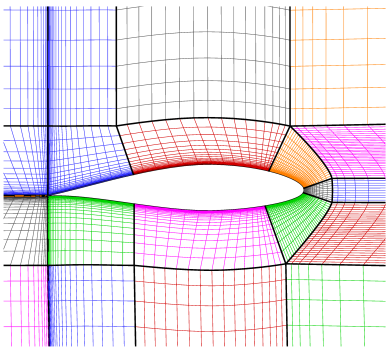

Figure 3. Multi-block grid around one of the blade sections.

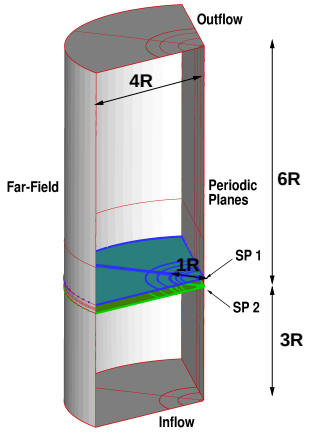

Figure 4. Single-blade computational domain, showing the boundary conditions and the extend of the domain. 2 sliding planes included for wake resolution.

4. Results and discussion

In all computed cases, axial wind conditions were assumed and the blade pitch angle was always set to $\phi = -2.3$ degrees. The turbulence model employed is the standard k-ω [19]. Table 3 summarises the main features of the computed cases.

Table 3. Computed test cases.

Test ID	Grid	Re	V_{wind}	$M_{tip}(\lambda)$	Aeroelastics	Low-Mach
1	1	$1.6 \cdot 10^6$	15	0.2941(6.67)	no	no
2	1	$1.6 \cdot 10^6$	15	0.2941(6.67)	yes	no
3	1	$1.6 \cdot 10^6$	15	0.2941(6.67)	no	yes
4	2	$1.6 \cdot 10^6$	15	0.2941(6.67)	no	no
5	2	$1.6 \cdot 10^6$	15	0.2941(6.67)	no	yes

4.1. Aeroelastic effects

A structural model of the MEXICO blade was put together using data from the MEXICO project reports documenting the manufacturing of the blade [16, 17]. The stiffness of the blade was based on assumed data for 7075 aluminium series. It should be noted that the torsional stiffness parameter J of each blade section was not defined. Hence, two different approaches are adopted: taking the minimum between the flapwise and edgewise inertias $min(I_{i,j})$, and average $avg(I_{i,j})$. Figure 5 shows the model that includes 20 elements of the CBEAM type of NASTRAN[20] (red) and several rigid bar elements (green) used to allow for better mapping between the CFD and FEM grids. This model was used for the static analysis of the blades, with

aerodynamic loads generated using CFD (*Test 1*). The exchange of loads between NASTRAN and the CFD solver is taking place several times during the computations until the shape of the blade and the aerodynamic loads converge to a final value, as described in [18].

Figures 6 (a) and (b) show the sensitivity of the torsional stiffness parameter to the predicted blade deformation in bending and torsion, for the two approaches previously mentioned and including variations of $^{+}_{-}10\%$. As can be seen, the bending is slightly dependent on the stiffness modulus (variation of less than $1cm$ from one approach to the other), while the torsional deflection is highly influential. This leads to high deflections when the minimum value is taken and small when the inertias are averaged, 3.5° and 0.225° of torsion at the tip, respectively. The resulting effective incidence angle for both cases is shown in Figure 7. This high dependence is observed in Figure 8, where a comparison between the rigid and deformed blades at five blade stations is presented. As can be seen, the aeroelastic effects are present from mid-span to the outboard stations.

Clearly, the torsional stiffness can influence the aerodynamic results. Further work is however needed to characterise the structural behaviour of the MEXICO blade so that the exact effect of the blade aeroelasticity is quantified.

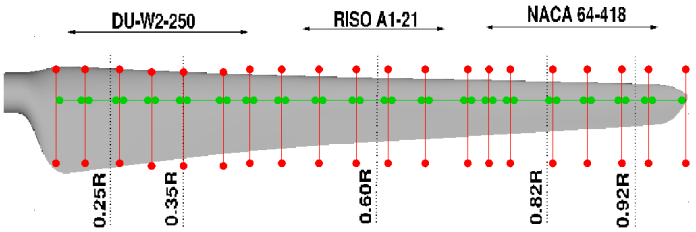

Figure 5. Structural model for the MEXICO blade.

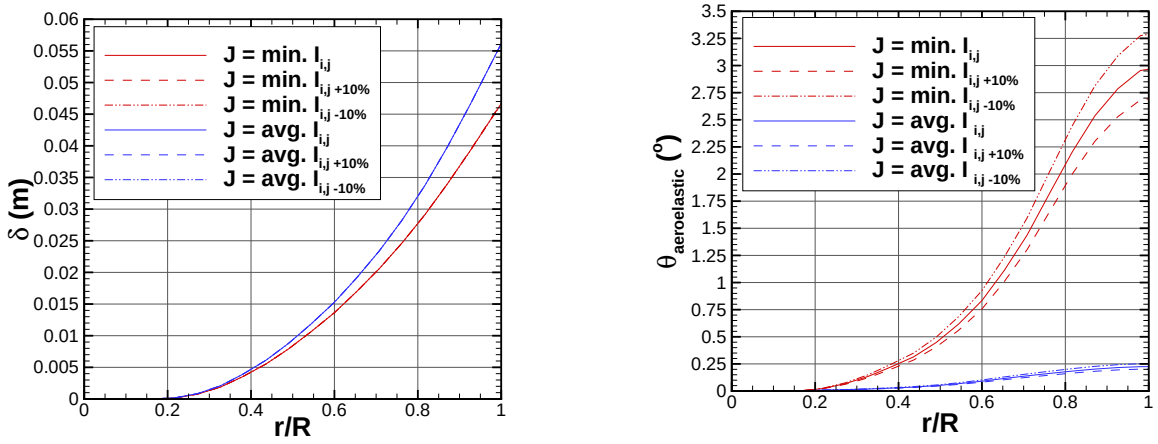

(a) (b)

Figure 6. Influence of the torsional stiffness magnitude on the (a) bending and (b) torsional deflection along the blade, due to aeroelastic effects using to J definitions (sensitivities of $^{+}_{-}10\%$ included). Red lines: minimum value of inertias ($J = I_2$), Blue lines: average between inertias ($J = \frac{I_1+I_2}{2}$).

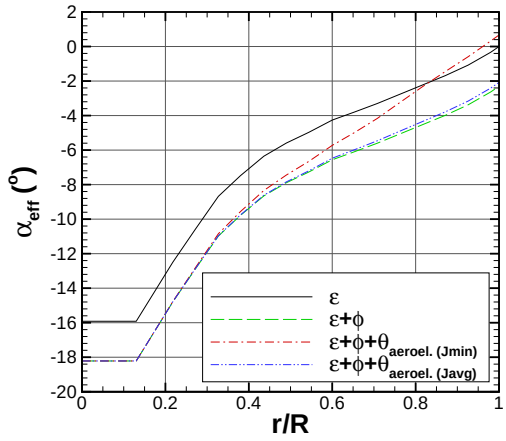

Figure 7. Influence of the torsional stiffness magnitude on the effective incidence angles along the blade (ϵ: twist angle, ϕ: pitch angle, $\theta_{aeroel.}$: torsional deflection due to aeroelastic effects). $J_{min} = I_2$ and $J_{avg} = \frac{I_1+I_2}{2}$.

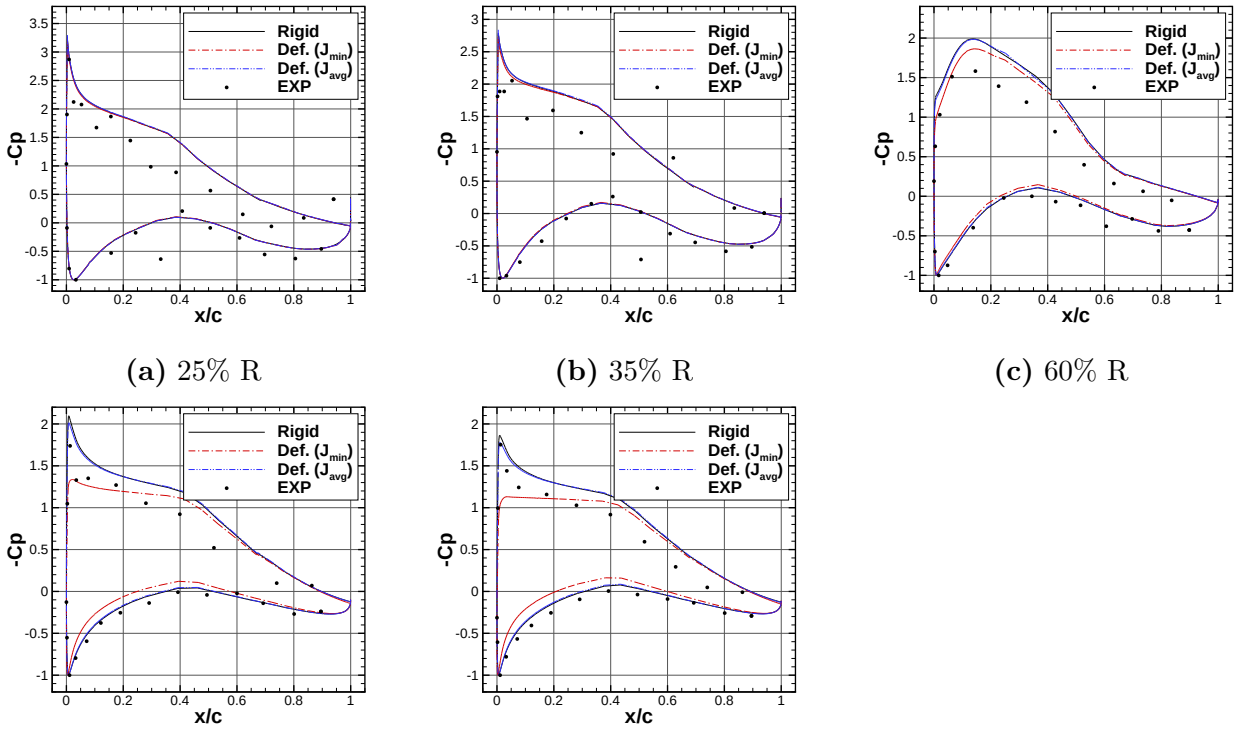

(a) 25% R **(b)** 35% R **(c)** 60% R

(d) 82% R **(e)** 92% R

Figure 8. Comparison of the C_p distribution between the rigid and the deformed blade ($J_{min} = I_2$ and $J_{avg} = \frac{I_1+I_2}{2}$) for *Test 1*: steady, $Re = 1.6 \cdot 10^6$, $V_{wind} = 15m/s$, $M_{tip} = 0.2941$.

4.2. Low-Mach effects

For this study, tests 1 and 3 are computed, consisting of steady cases at a Reynolds number of 1.6 million and tip Mach number of 0.2941. A comparison between the Osher's [21], the standard Roe [22] and the LM-Roe [23] schemes is presented in Figure 9, where the computed

pressure coefficients at five radial stations are plotted against the experimental data. As can be seen, the solution obtained with all three schemes is very similar. O-Roe and Osher results are almost identical, while the LM-Roe scheme gave slightly lower values on both pressure and suction sides. However, the differences between the three schemes are minimal. This is due to the fact that, for this test case, the Mach numbers encountered around the blade are not low enough for the low-Mach effects to be important.

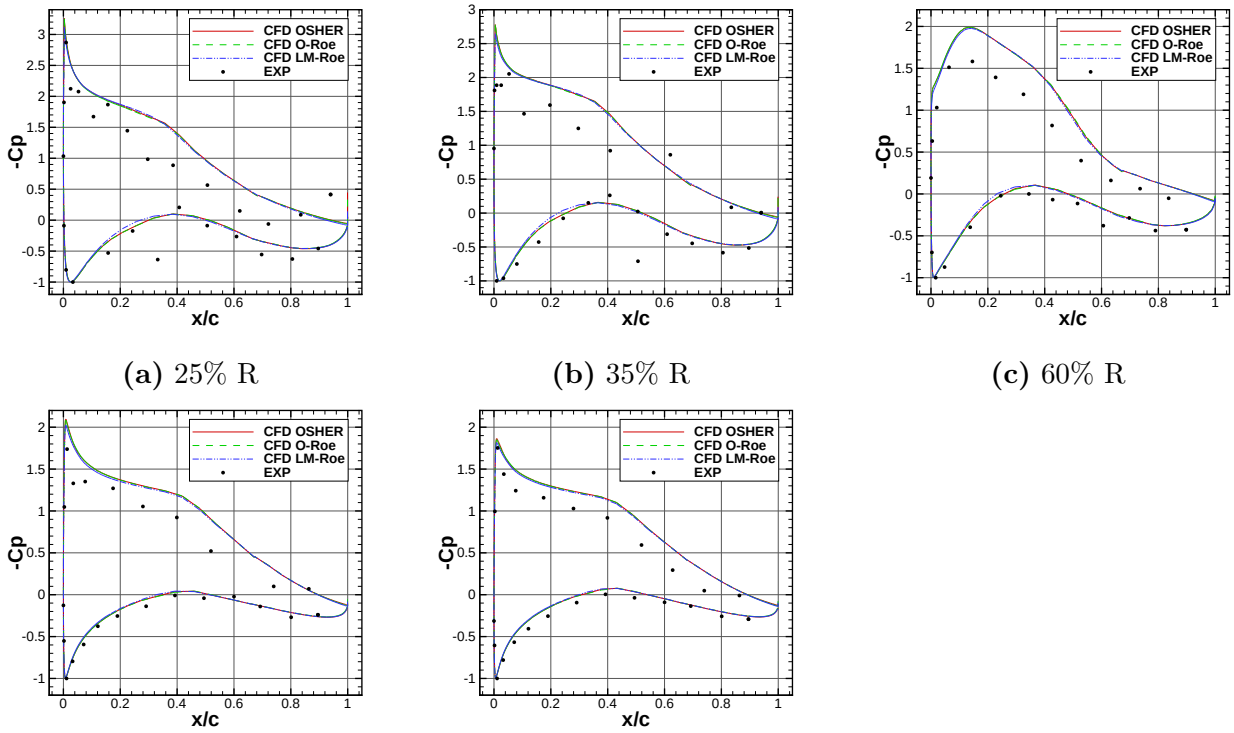

(a) 25% R **(b)** 35% R **(c)** 60% R

(d) 82% R **(e)** 92% R

Figure 9. Comparison of the C_p distribution between Osher [21], standard Roe [22] and LM-Roe [23] schemes for *Test 3*: steady, $Re = 1.6 \cdot 10^6$, $V_{wind} = 15m/s$, $M_{tip} = 0.2941$.

4.3. Velocity field

In this section, the velocity field behind the wind turbine is discussed. Steady computations using the standard Osher and Low-Mach Roe solvers, at the conditions of Table 3, Tests 3 and 4, are compared against the Particle Image Velocimetry data of the wind tunnel campaign [26].

Figure 10 shows the three components of the velocity profiles at two radial stations: 60%R and 82%R. Regarding the axial component (Figures 10 (a) and (d)) higher velocities are observed in the computations, suggesting that the inflow wind speed velocity in the experiments was lower than $15m/s$. However, the values obtained with the LM-Roe scheme seem to get closer to the experiments. On the other hand, the oscillatory pattern on the span-wise component (Figures 10 (b) and (e)) is well captured by both schemes, with better agreement found at 82%R. This is due to grid refinement, since the smaller cells were set between 75%R and 140%R. A similar behaviour is observed for the tangential component (Figures 10 (c) and (f)), where both schemes gave similar solutions. Nevertheless, an improved grid of higher resolution is necessary for further computations.

Finally, Figure 11 shows contours of the three velocity components with the blade at an azimuth angle of 270 degrees, where the position of the vortex can be observed. For the three components, the agreement with experiments is slightly better with the LM-Roe scheme than with the Osher. This is due to a somehow less dissipative nature of the low-Mach solution. The position of the vortex core is well-predicted and any expansion of the core is due to the coarse mesh employed.

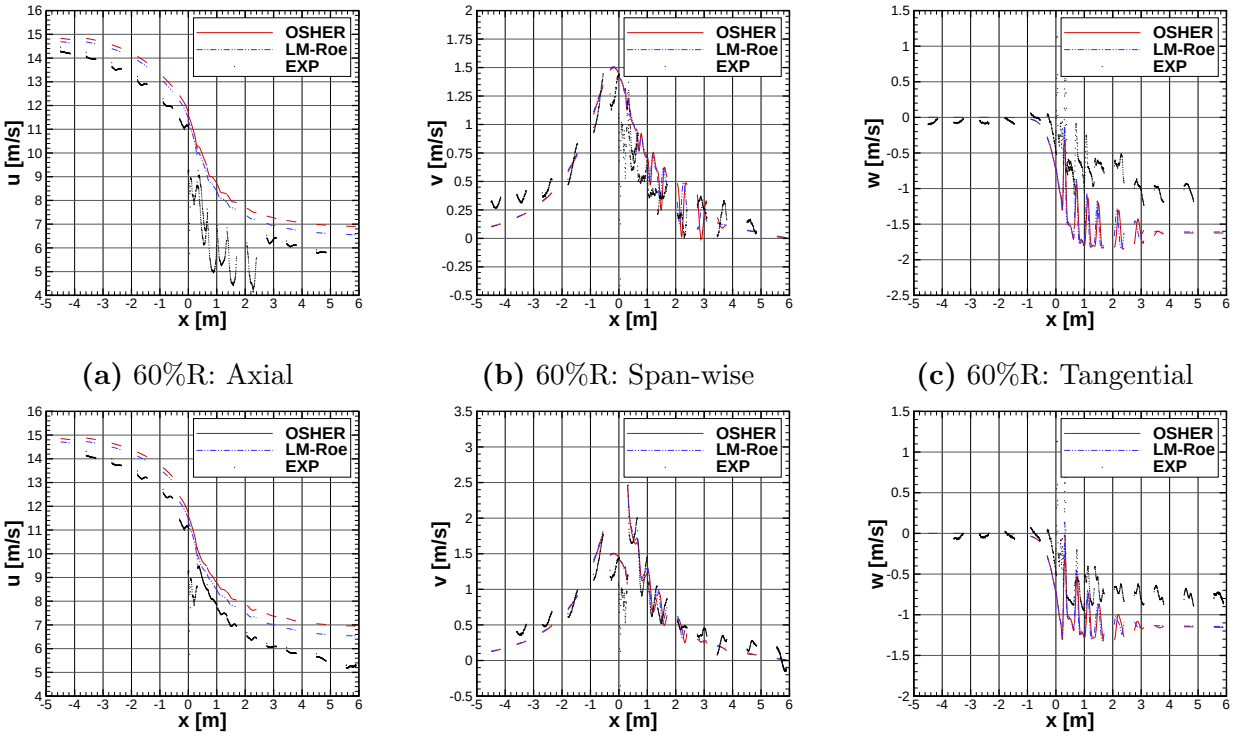

(a) 60%R: Axial **(b)** 60%R: Span-wise **(c)** 60%R: Tangential

(d) 82%R: Axial **(e)** 82%R: Span-wise **(f)** 82%R: Tangential

Figure 10. Comparison of the axial, span-wise and tangential velocity profiles at Top: 60%R and Bottom: 82%R. The wind speed is $15m/s$ and the blade is at 270 degrees of azimuth angle.

5. Conclusions and future work

Computing the third of the rotor using periodic formulation in steady-state proved to be very efficient, since the computations were less time-consuming and the grid size was reduced. Regarding the blade aeroelasticity, high dependence on the torsional stiffness was observed. Nevertheless, the aeroelastic method performed well and the structural model can always be reused based on new data for the torsional stiffness. The obtained results showed that low-Mach effects on the blade loading were minimal. On the other hand, computations with a finer grid enabled to study the velocity field behind the rotor and showed good agreement with experiments. Likewise, the low-Mach scheme seemed to capture the wake better.

In the future, efforts will be directed in extending the study to cover low-Mach, aeroelastic and wind tunnel effects, as well as computing different wind conditions.

Acknowledgments

The financial support by the Spanish Renewable Energy Center (CENER) and the University of Liverpool is gratefully acknowledged.

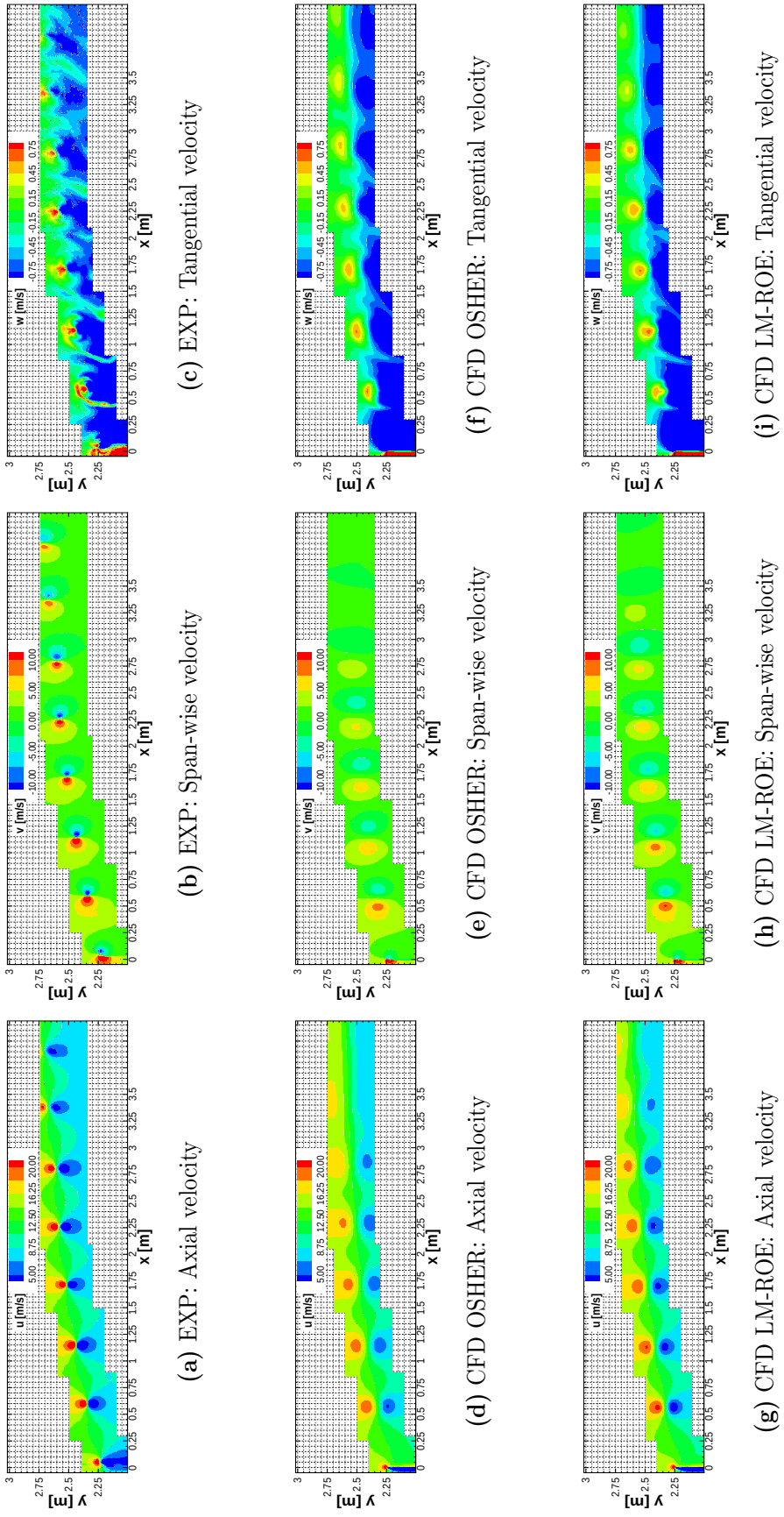

(a) EXP: Axial velocity (b) EXP: Span-wise velocity (c) EXP: Tangential velocity

(d) CFD OSHER: Axial velocity (e) CFD OSHER: Span-wise velocity (f) CFD OSHER: Tangential velocity

(g) CFD LM-ROE: Axial velocity (h) CFD LM-ROE: Span-wise velocity (i) CFD LM-ROE: Tangential velocity

Figure 11. Contours of the axial, span-wise and tangential velocity components, for wind speed of $15m/s$ and blade at 270 degrees of azimuth angle.

References

[1] S.J. Lawson, R. Steijl, M. Woodgate, and G.N. Barakos, *High Performance Computing for Challenging Problems in Computational Fluid Dynamics*, Progress in Aerospace Sciences, Vol. 52, pp. 19-29, July 2012, DOI 10.1016/j.paerosci.2012.03.004.

[2] R. Steijl, G.N. Barakos, *CFD Analysis of Complete Helicopter Configurations Lessons Learnt from the GOAHEAD Project*, Aerospace Science and Technology, Vol. 19, Issue 1, pp. 58-71, June 2012, DOI 10.1016/j.ast.2011.01.007.

[3] M. Woodgate, and G.N. Barakos, *Implicit CFD Methods for Fast Analysis of Rotor Flows*, AIAA Journal, Vol. 50, Issue 6, pp. 1217-1244, June 2012, DOI 10.2514/1.J051155

[4] F. Dehaeze and G.N. Barakos, *Mesh Deformation Method*, AIAA J. of Aircraft, Vol 49, Issue 1 (January-February 2012).

[5] C. Johnson, and G.N. Barakos, *A Framework for Optimising Aspects of Rotor Blades*, The Aeronautical Journal, Vol. 115, Issue 1165, pp. 147-161, March 2011.

[6] R. Steijl and G.N. Barakos, *Computational Study of Helicopter Rotor-Fuselage Aerodynamic Interaction*, AIAA Journal, Vol. 47, Issue 9, pp. 2143- 2157, September 2009.

[7] A. Gagliardi and G.N. Barakos, *Analysis and Design of a Flap-Equipped Low-Twist Rotor for Hover*, AIAA Journal of Aircraft, 46(1), pp. 74-84, January-February 2009, DOI 10.2514/1.34275.

[8] S. Gomez-Iradi, R. Steijl and G.N. Barakos, *Development and Validation of a CFD Technique for the Aerodynamic Analysis of HAWT*, J. Solar Energy Engineering-Transactions of the ASME, 131(3):031009, 2009. DOI: 10.1115/1.3139144.

[9] R. Steijl and G.N. Barakos, *Sliding Mesh Algorithm for CFD Analysis of Helicopter Rotor-Fuselage Aerodynamics*, International Journal for Numerical Methods in Fluids, 58(5), 527-549, October 2008, DOI: 10.1002/d.1757.

[10] R. Steijl, G.N. Barakos and K. Badcock, *Computational Study of the Advancing-Side Lift-Phase Problem*, AIAA Journal of Aircraft, 45(1), 246-257, January-February 2008, DOI: 10.2514 / 1.22044.

[11] R. Steijl, G.N. Barakos and K. Badcock, *A Framework for CFD Analysis of Helicopter Rotors in Hover and Forward Flight*, International Journal for Numerical Methods in Fluids, 51(8), 819-847, July 2006, DOI 10.1002 / d.1086.

[12] G.N. Barakos, R. Steijl, A. Brocklehurst and K Badcock, *Development of CFD Capability for Full Helicopter Engineering Analysis*, 31st European Rotorcraft Forum, Florence, Italy, 13-15 September 2005.

[13] F. Harlow and J.E. Welch, *Numerical Calculation of Time-dependent Viscous Incompressible Flow of Fluid with a Free Surface*, Physics and Fluids. 8 (1965) 21829.

[14] L. Dubuc, F. Cantariti, M.A. Woodgate, B. Gribben, K.J. Badcock and B.E. Richards, *A Grid Deformation Technique for Unsteady Flow Computations*, International Journal for Numerical Methods in Fluids, Vol.32, p.285-311, 2000.

[15] O. Axelsson, *Iterative Solution Methods*, Cambridge University Press: Cambridge, MA, 1994.

[16] A. Rosen, A. Wolf, D. Ben-Shmuel and G. *Part I. The MEXICO Project Wind Turbine Model*, TAE No. 985, Technion Research and Development Foundation, August 2011.

[17] A. Rosen, A. Wolf, D. Ben-Shmuel and G. Omri, *Part II. The MEXICO Project Wind Turbine Model*, TAE No. 986, Technion Research and Development Foundation, August 2011.

[18] F. Dehaeze and G.N. Barakos, *Hovering Rotor Computations Using an Aeroelastic Blade Model*, Aeronautical Journal, Vol. 116, Issue 1180, pp. 621-649, June 2012.

[19] D.C. Wilcox, *Multi-scale Model for Turbulent Flows*, AIAA Journal, vol.26, Issue 11, p.1311–1320, 1988.

[20] MSC.Software Corporation, *MSC.Nastran 2005 Release Guide*, Macmillan, 2005.

[21] S. Osher and S. Chakravarthy, *Upwind Schemes and Boundary Conditions with Applications to Euler Equations in General Geometries*, J. Comp Phys. 50 (1983) 447–481.

[22] P.L. Roe, *Approximate Riemann Solvers, Parameter Vectors, and Difference Schemes*, J. Comp. Phys. 43 (1981) 357–372.

[23] F. Rieper, *A Low-Mach Number Fix for Roe's Approximate Riemann Solver*, J. Comput. Phys. 230 (2011) 5263–5287.

[24] M. Carrión, M. Woodgate, R. Steijl and G. Barakos, *Implementation of All-Mach Roe-type Schemes in Fully Implicit CFD Solvers - Demonstration for Wind Turbine Flows*, International Journal for Numerical Methods in Fluids, 2013, DOI: 10.1002/fld.3818.

[25] X.S. Li and C.W. Gu, *An All-Speed Roe-type Scheme and its Asymptotic Analysis of Low Mach Number Behaviour*, J. Comput. Phys. 227 (2008) 5144–5159.

[26] H. Snel, J.G. Schepers and B. Montgomerie, *The MEXICO project (Model Experiments in Controlled Conditions): The database and first results of data processing and interpretation.*

[27] D.M. Somers, *Design and experimental results for the S809 airfoil*, In Subcontract Report SR-440- 6918, NREL, Colorado, USA, January 1997.

[28] R.R. Ramsay, M.J. Hoffmann, G.M. Gregorek, *Effects of Grit Roughness and Pitch Oscillations on the S809 Airfoil*, National Renewable Energy Laboratory, Golden (1995).
[29] A. Bechmann, N.N. Sorensen, and F. Zahle, *CFD Simulations of the MEXICO Rotor*, Wind Energy, vol.14, Issue 5, p.677–689, July 2011.
[30] H. Yang, W.Z. Shen, J.N. Sorensen and W.J. Zhu, *Extraction of airfoil data using PIV and pressure measurements*, Wind Energy, vol.14, Issue 4, p.539–556, May 2011.
[31] W.Z. Shen, and W.J. Zhu, and J.N. Sorensen, *Actuator Line/Navier-Stokes Computations for the MEXICO Rotor: Comparison with Detailed Measurements*, Wind Energy, DOI: 10.002/we.510, 2011.
[32] W. Xudong, W.Z. Shen, W.J. Zhu, J.N. Sorensen and C. Jin, *Shape Optimization of Wind Turbine Blades*, Wind Energy, vol.12, Issue 8, p.781-803, March 2009.
[33] S.P. Breton, C.S. Watters, C. Masson, S. Gómez-Iradi, X. Munduate, *On the Prediction of Tip Vortices in the Near Wake of the MEXICO Rotor using the Actuator Surface Method*, Engineering Systems Modelling and Simulation, vol. 4, p.11-26, 2012.
[34] D. Micallef, G. van Bussel, C.S Ferreira, T. Sant, *An Investigation of Radial Velocities for a Horizontal Axis Wind Turbine in Axial and Yawed Flows*, Wind Energy, DOI: 10.1002/we.1503, 2012.
[35] R. Pereira, G. Schepers and M.D. Pavel, *Validation of the Beddoes-Leishman Dynamic Stall Model for Horizontal Axis Wind Turbines using MEXICO data*, Wind Energy, DOI: 10.002/we.541, 2012.
[36] T. Lutz, *Near Wake Studies of the MEXICO Rotor*, EWEA Annual Event, March 2011.
[37] F. Grasso and A. van Garrel, *Near Wake Simulation of MEXICO rotor in Axial and Yawed Flow Conditions with Lifting Line Free Wake Code*, Wake Conference, June 2011.
[38] P.E. Réthoré, N.N, Sorensen, F. Zhale, A. Bechmann, H.A. Madsen, *CFD model of the MEXICO Wind Tunnel*, EWEA Annual Event, March 2011.
[39] P.E. Réthoré, N.N, Sorensen, F. Zhale, A. Bechmann, H.A. Madsen, *MEXICO Wind Tunnel and Wind Turbine modelled in CFD*, AIAA Conference, June 2011.
[40] D. Micallef, M. Kloosterman, C.S Ferreira, T. Sant and G. van Bussel, *Validating BEM, Direct and Inverse Free Wake Models with the MEXICO experiment*, 48th AIAA Aerospace Sciences meeting, January 2010.
[41] S. Schreck, T. Sant and D. Micallef, *Rotational Augmentation Disparities in the UAE Phase VI and MEXICO Experiments*, Torque from Wind Conference, June 2010.
[42] K. Guntur, C. Bak, C. Niels and N.N. Sorensen, *Analysis of 3D Stall Models for Wind Turbine Blades using Data from the Mexico Experiment*, 13th Int. Conf. on Wind Engineering, ICWE, July 2011.
[43] S. Gómez-Iradi, X. Munduate and A. Irisarri, *Task 4.1 - Standstill*, MexNext Meeting, Amsterdam, Netherlands, January 2011.
[44] S. Gómez-Iradi and X. Munduate, *A CFD Investigation of the Influence of Trip-Tape on the MEXICO Wind Turbine Blade Sections*, The science of making torque from wind, 2011.